TESTING CRUSTAL VOLATILE REMOBILISATION

Sylvia E. Berg

Department of Earth Sciences, Uppsala University (www.geo.uu.se)
Nordic Volcanological Center, University of Iceland (www.nordvulk.hi.is)

This project that has been undertaken in Pisa during September 2012 forms part of a larger study on frothy xenolith pumices, coordinated by Prof. Valentin R. Troll (CEMPEG, Uppsala University). This study covers geochemical, gas chemical, and HP-HT (high pressure-high temperature) experimental work on magma-crust interaction, combined with synchrotron radiation X-ray computed microtomography (μ-CT) information. A key aim of this wider study is to test processes of crustal volatile remobilisation, which, in part, involves tracing gas release and volatile migration through crustal xenoliths (see Fig. 1). This particular project here focuses on information gained from X-ray μ-CT imaging from experiments performed at the Elettra Synchrotron Light Laboratory in Trieste (Italy), which offers three dimensional (3D) insights into vesicle densities, vesicle shapes and vesicle networks. This provides unique insights into reactions and volatile remobilisation processes during magma-crust interaction.

In collaboration with Dr. Margherita Polacci at the host institute, INGV in Pisa, we have analysed the very recently erupted crustal xenoliths from El Hierro, Canary Islands, in October 2011 (Troll et al., 2012). The El Hierro submarine eruption emitted intriguing eruption products during its early eruptive phase, which were found floating in the sea. These were termed “restingolites” (after the close-by village La Restinga) and exhibit cores of white and porous pumice-like material, covered by glassy, basanitic crusts (see Fig. 1). The nature and origin of these “floating stones” were vigorously debated among researchers, with important implications for the interpretation of the hazard potential of the ongoing eruption. However, Troll et al. (2012) gives textural, mineralogical and geochemical evidence that these are in fact xenoliths from pre-island sedimentary rocks that were picked up and heated by the ascending magma, causing them to partially melt and vesiculate. They are likely prime examples of magma-crust interaction.

In November 2011 four specimens from the 2011 El Hierro submarine eruption were analysed by non-destructive, high-resolution X-ray μ-CT at the Tomolab and the SYRMEP beamline at the Elettra Synchrotron Light Laboratory in Trieste (Italy). This X-ray μ-CT digital dataset has been processed and modelled with freeware ImageJ (Abramoff, 2004), the commercial software VGStudio MAX 2.0 and the Pore3D library (Brun et al., 2010). This approach has allowed internal textural visualisation of the specimens in 3D, and quantitative studies of internal vesicle volumes, networks and connectivity in 3D. Together this gathered information has offered unprecedented insight into mechanisms during partial melting and gas release in these crustal lithologies during volcanic magma-crust interaction.

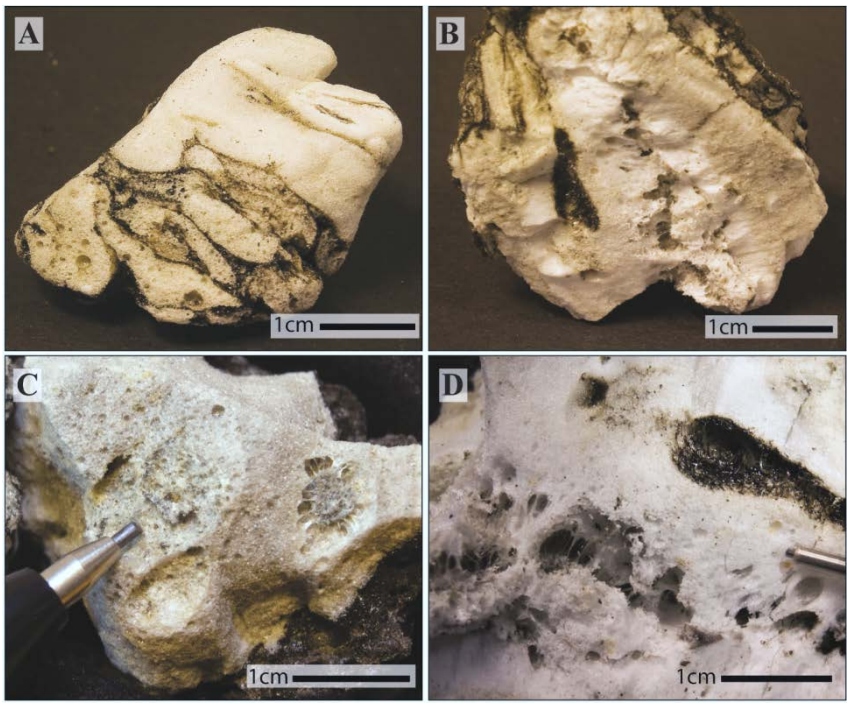

Figure 1. Hand specimens of foamed xenoliths from El Hierro 2011 (see Troll et al., 2012). A) Mingling structures as basanite mix with white sediment. B) Vigorous vesiculation in the interior of the sediment. C) and D) close-up of vesicles, and relics (in C).

APPROACH – *SEGMENTATION AND VOI*

Processing of the 2D digital dataset obtained from X-ray μ-CT into final 3D renderings and quantitative analyses of the samples requires several intermediate steps that are necessary to obtain representative results at the end. The first procedure is segmentation of the images, which involves image enhancements to improve the final output image, and may also involve a few manipulations of some intermediately computed image descriptors (Fig. 2 and summary Fig. 5).

The majority of image analysis approaches requires a segmentation step, which can be considered as the "bridge" between the image processing and image analysis fields. There is no single standard segmentation procedure, but it has to be applied in consideration to the type of object in question. The chosen segmentation procedure applied on our xeno-pumice samples is briefly described here. This involves image segmentation by thresholding, creating a binary image by separating voxels into either "object" voxels, if their value is greater than some specified threshold value (assuming the object to be brighter than the background), and as "background" voxels otherwise. In our samples this approach separates "air" (pore spaces) in the sample from solid parts (glass, crystal relics etc.). Good segmentation is a crucial step for further image analyses of the porous media. The selection of a good and representative threshold value was performed by a *trial and error* assessment, via visual evaluation of the results produced by a few trials with different threshold values.

Additional steps were also part of the segmentation to improve the thresholding process. Both pre- and post-segmentation filters were applied. An image enhancement smoothing filter was applied to the grey-scale input image in order to ease the thresholding. After careful consideration and testing of several different filters, the most appropriate filter for our samples proved to be the anisotropic diffusion model. This is one of the edge-preserving smoothing filters (Perona and Malik, 1990), which aims at smoothing regions without affecting object edges. Post-segmentation techniques include the application of a binary filter that processes the "black and white" representation of the output image. Image noise like islands of voxels in the pore spaces were removed by simple post-segmentation techniques that eliminate connected components (i.e. an isolated cluster of object voxels) having

volume (i.e. number of voxels) below a specified threshold value (Soille, 2004). This threshold value was determined from careful testing via the *trial and error* assessment for each sample.

Prior to the segmentation step an accurate selection of the VOI (Volume of Interest) for the image analysis process is performed in order to simplify the actual segmentation. In general, the selected VOI should be small enough to be easily handled by the available computer hardware but at the same time large enough to comprehend all the representative features of the sample. As a rule of thumb the selected VOI should have a size about one order of magnitude larger than the characteristic size of the underlying structure (e.g. the mean size of the studied objects or pores in the sample) (Ohser and Schladitz, 2009). The VOI is also selected in relation to image quality, trying to avoid artifacts in the sample that would complicate further analyses. Normally the VOI was selected in the middle of the sample.

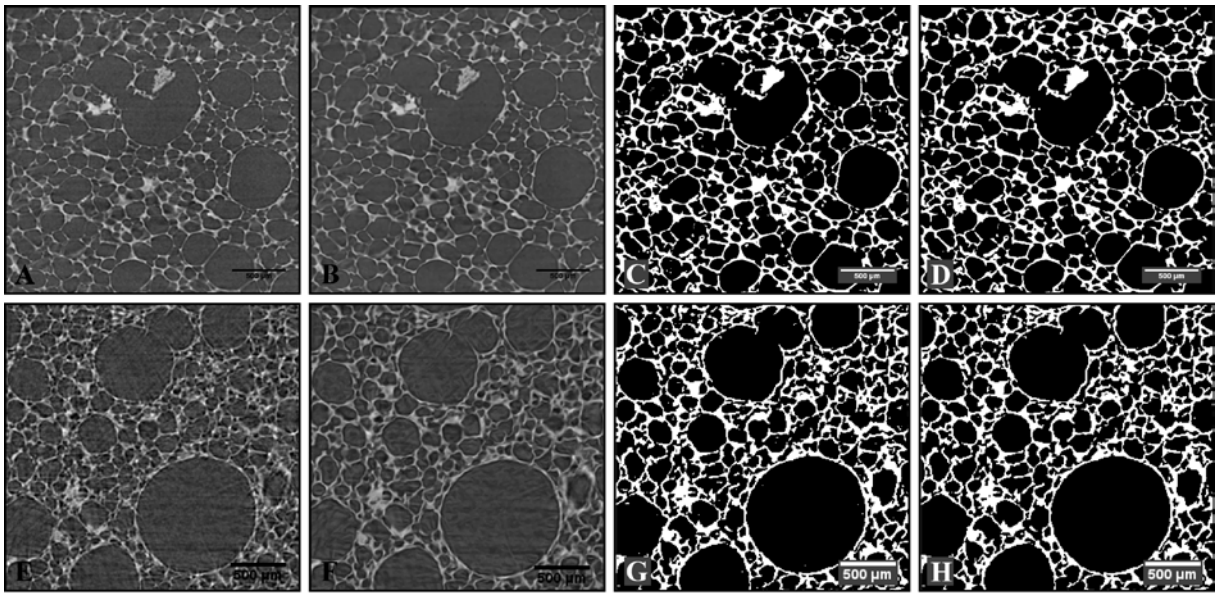

Figure 2. Image sequence of segmentation procedure. A-D) Sample EH-XP-10LA, E-H) sample EH-XP-2-right. A) and E) raw images, B) and F) anisotropic diffusion filter applied, C) and G) thresholded binary image, D) and H) final output images, filtered to remove small islands of voxels.

IMAGE ANALYSIS

Three-dimensional image analysis of these porous xeno-pumice samples from El Hierro were performed with Pore 3D (Brun et al. 2010); the output data were then modeled and interpreted in 3D with VGStudio MAX 2.0. The results are all relying on the fact that the "best" possible segmentation was obtained for the sample, because even just a slight change in the chosen threshold value would change the data output.

A first order of simple image descriptor applied is volume fraction or density (V_V). The volume density simply represents the density of the segmented sample, i.e. the number of voxels belonging to the object phase with respect to the total number of voxels in the considered VOI. The measure ($1-V_V$) represents the density of the complementary phase and it is usually denoted as porosity if the complementary phase is the pore space (see result section, Table 1).

Another descriptor applied is labeling of connected components, which results in a separation of isolated blobs and connected components/blobs. Obviously this approach works best for a set of

isolated blobs and less so for a system of complexly connected blobs, i.e. a vesicle network. However, labeling will give a representation of the vesicle connectivity, which is important to understand vesicle networking processes in the sample. If the pore space is formed by a set of isolated "blobs", a series of descriptors for size and shape of each "blob" can be computed, like volume, minor and major axis, sphericity, diameter of the maximum inscribed sphere, equivalent diameter (specifies the diameter of a sphere with the same volume as the blob), aspect ratio etc. Though, for high porosity samples with whole (or partial) vesicle interconnection, this approach would not offer representative information as isolated vesicle cannot be easily recognised. This is because e.g. the closed cells often present very thin walls of a size below the spatial resolution of the adopted imaging technique. For a few of the samples analysed this was the case, Pore3D was able to detect one big vesicle/pore and only a few isolated pores (see Fig. 3), whereas in reality it probably existed a small percent of more small isolated pore spaces in the sample.

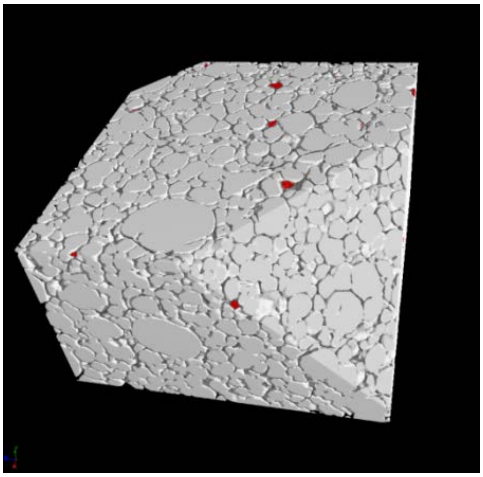

Figure 3. Sample EH-XP-10LA described with a labeling algorithm that demonstrates a small number of isolated vesicles (red) whereas all the remaining vesicles are connected in 3D (grey).

SKELETON ANALYSIS OF OPEN PORE SPACES

To quantify and visualise the degree of pore interconnection in porous samples a skeletonization algorithm is applied, which allows quantifying size and shape of the pores composing the pore space. An extracted skeleton from the binary 3D image is a description of the binary object in terms of nodes and branches (Lindquist and Lee, 1996). A node is defined as the point of intersection of two or more skeleton branches, a branch is either a connection node-to-node or a node-to-end branch.

Several different skeletonization algorithms exist, and each may give different output results. In general, the skeleton is a set of idealised connected thin lines that preserve the original topology and captures both boundary and region information, forming a set of nodes and branches that represent the medial axis of the object. Here we applied the GVF (Gradient Vector Flow) skeletonization algorithm that was introduced by F. Brun (Brun and Dreossi, 2010). This algorithm benefits from the fact that it produces a thin and centered curve-skeleton also in presence of noisy objects (like islands of voxels etc.), which is common in very densely vesiculated samples.

Further skeleton analysis allows quantifying the number and the dimensions of nodes and branches, and also measurements of pore and throat thickness, based on the concept of maximal inscribed sphere (Hildebrand and Rüegsegger, 1997). This concept is based on the inflation of a sphere centered at a skeleton node (Fig. 4 and 6G). The inflation continues until the sphere "touches" the walls of the pore space. Hence, the diameter of this maximal inflated sphere gives a representative estimation of the pore size and also pore size distribution in the sample before pores were connected. The same approach can also be used for the skeleton branches. The minimum thickness along such a skeleton branch would then be denoted as the minimum size of the channel or the throat connecting the pores. For an interconnected pore space there is no explicit method to geometrically define where a pore ends and a connecting channel begins, making a pore and throat separation slightly difficult. Conceptually, all nodes would correspond to pore bodies, while the branches represent channels connecting the pores. Imperfect skeletonization may however disturb this correspondence, e.g. several nodes may occur in the same pore body and not every branch may corresponds to a channel as short branches

between two nodes actually would still be considered as part of the pore. This has to be considered during quantitative analyses and, if considered important, several correction criterions can be applied.

One of the parameters produced from skeleton analysis is the pore coordination number (i.e. the number of channels (skeleton branches) connected to a pore (skeleton node). The mean coordination number for the whole skeleton can then serve as characterisation of pore space connectivity.

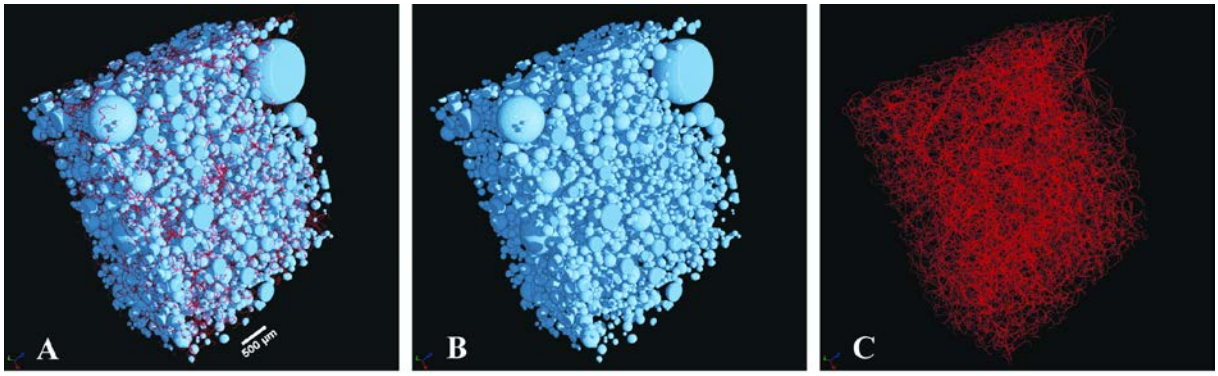

Figure 4. Sample EH-XP-10LA, A) Skeleton (red) and inflated pores (blue) at skeleton nodes. B) Inflated pores only. C) Skeleton.

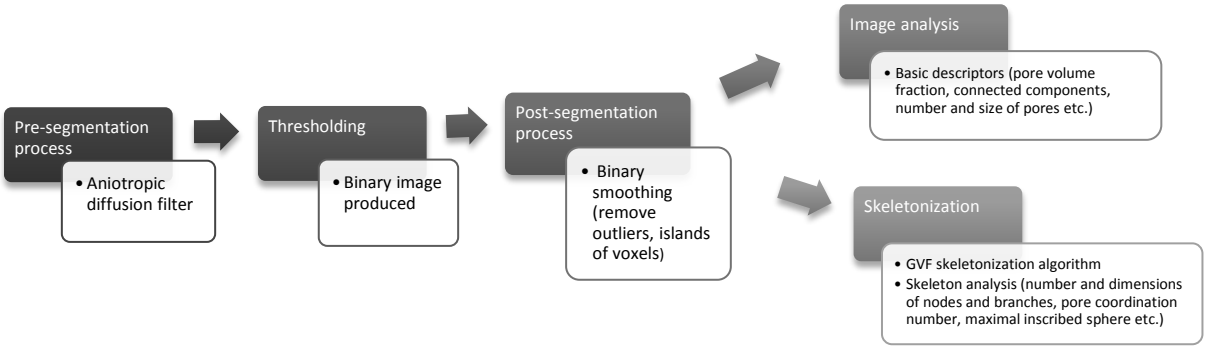

Figure 5. Schematic procedure of segmentation and image analyses.

MAIN RESULTS

Three-dimensional renderings of each analysed sample offer instructive visualisation of the xeno-pumices, enabling to interpret their history of formation, as well as, processes during magma-crust interaction (see Fig. 6). In addition, quantitative image analyses also provide measurements of the pore space in the sample. The volume fraction of the pore space in the VOI is calculated and then divided by the total VOI volume, giving sample porosity for each sample (Table 1). The connected component labeling of the pore space broadly provide an insight into the number of isolated pores as well as the connectivity between the pores (Fig. 3).

The skeleton offers a visual representation of pore interconnectivity and the maximal inscribed spheres at the nodes provide a size distribution of the pore volume in the sample, which gives an indication of the number of vesicle populations/generations before vesicles were interconnected (Fig. 4).

Table 1: Pore analyses

Sample	Experiment		Pixelsize (µm/px)	Height	Width	slices	Voxelsize (mm^3)	Threshold	Total pore volume (mm^3)	VOI (mm^3) (H *W*slices*voxel-size^3)	Porosity (%)	Number of isolated vesicle volumes
EH_XP_1	SYRMEP	Nov. 2011	9	256	370	400	7.29E-07	53	14.32	27.62	51.86	3
EH_XP_2_right	SYRMEP	Nov. 2011	9	317	370	400	7.29E-07	86	22.29	34.20	65.18	1
EH_XP_2_left	SYRMEP	Nov. 2011	9	236	274	454	7.29E-07	86	13.64	21.40	63.72	1
EH_XP_10	TOMOLAB	Sept. 2012	6.58	858	957	500	2.85E-07	75	79.74	116.96	68.18	48
EH_XP_10LA	TOMOLAB	Sept. 2012	5	544	290	500	1.25E-07	82	7.42	9.86	75.24	56
EH_XP_13	TOMOLAB	Sept. 2012	7.1	467	473	500	3.58E-07	71	17.57	39.53	44.44	895

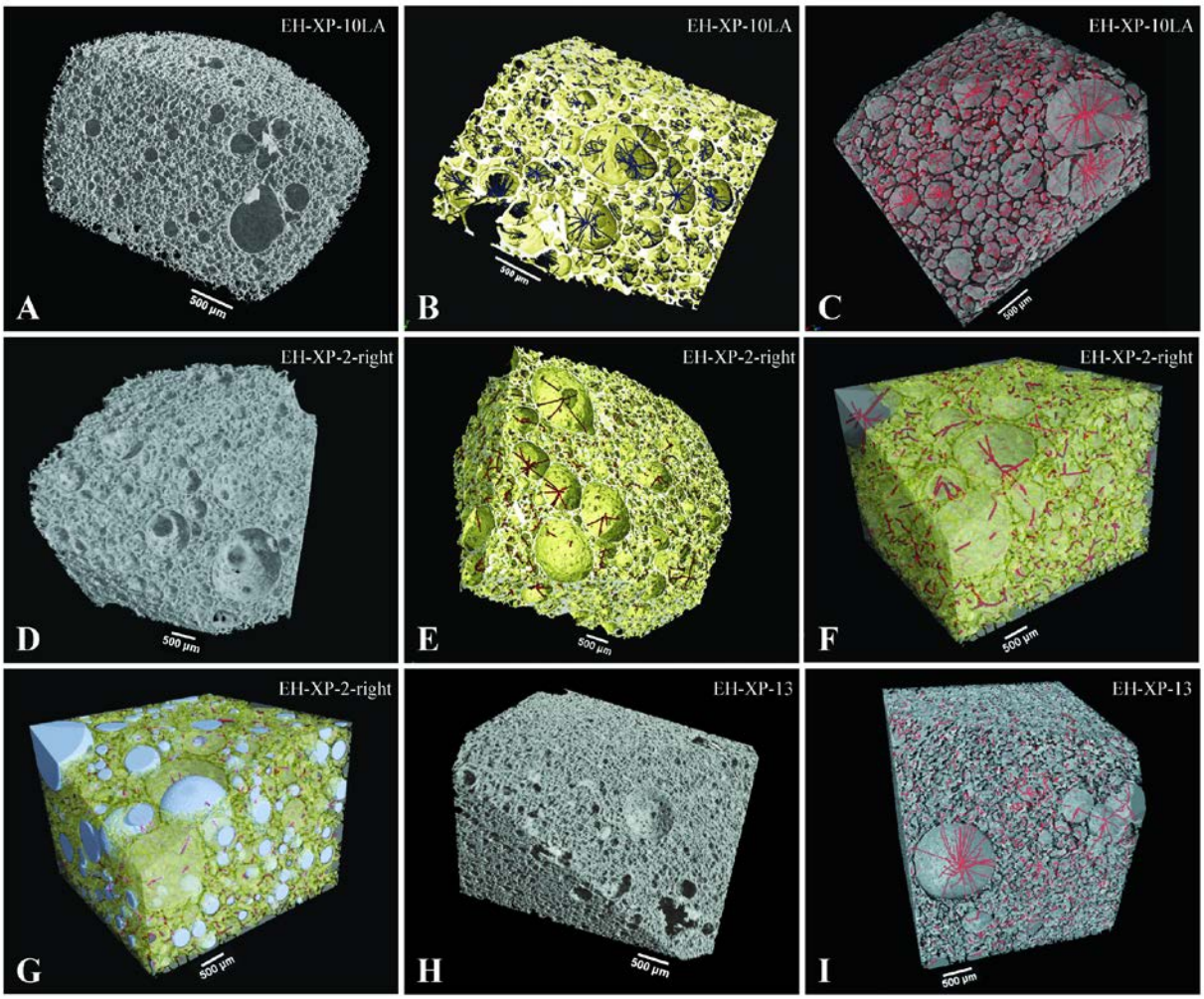

Figure 6. Volume renderings of selected samples. A) Solid rendering in grey. B) Solid rendering (yellow) and skeleton in blue. C) Isolated vesicle phase that appears slightly transparent, and the skeleton (red) can be traced from one vesicle to the other. D) Solid rendering in red. E) Solid rendering (yellow) and skeleton in red. F) Transparent vesicle phase with red skeleton. G) same as F) with inflated spheres at skeleton nodes. H) solid rendering (grey). I) Transparent vesicle phase with red skeleton, note tortuous small vesicles and large spherical vesicles.

DISCUSSION

The xeno-pumices from El Hierro are characterised by vesiculated textures, glass (former melt) and a few crystal relics. In general, vesicles can be divided into at least two size classes (each class reflecting a specific vesicle nucleation event). The larger vesicles measure from ~500 µm to ~1 mm in diameter, whereas the smaller vesicles range from ~100 µm to ~300 µm.

Volume renderings demonstrate an apparent textural difference between the samples, largely on vesicle size and shape (see fig. 6). Sample EH-XP-10LA has large vesicles that are slightly irregular to sub-spherical; the smaller vesicles are often close to spherical. In sample EH-XP-2-right both small and large vesicles are close to spherical. Sample EH-XP-13, on the other hand, has very tortuous small vesicles and a few big spherical vesicles. This is rather intriguing as, from a perspective of vesicle dynamics and also comparison with other volcanic pumice textures, the opposite is most often the case. Suggestively, the small tortuous vesicles could form during the latest stage of magma-xenopumice interaction, just prior to complete solidification and at a stage when the supersaturation pressure was so high that vesicles were not only restricted to spherical shapes that are the least energy demanding (e.g. Sparks, 1978; Cashman & Mangan, 1994; Hurwitz & Navon, 1994).

In general, samples display a polymodal vesicle size distribution with at least two vesicle generations. From pore labeling and careful observation of the vesicle skeleton the interconnection and networking between the vesicles are fairly high, even though the porosity reaches to about 75 % at the most, just barely surpassing the 74% limit that characterizes magmatic foams.

The textural dissimilarities between the samples that originate from the same sea sediments below the El Hierro island, indicate that the samples underwent varying reaction processes during magmatic entrainment. This may result from various magmatic residence times, depth of entrainment, magmatic activity (magmatic pulses of varying intensity during the eruption) etc., which affect vesicle nucleation and growth rates. In addition, it should be considered that samples were collected during different days of the eruption, and that the analysed samples may thus represent different parts of the reaction process, i.e. rim and core are affected differently with respect to magma proximity.

FUTURE COLLABORATION

The collaboration between Dr. Polacci from INGV-Pisa and Uppsala University, where Sylvia Berg is doing her PhD studies, will continue in the future with the analysis and interpretation of xeno-pumice products coming from different volcanic areas and tectonic/magmatic environments. This will enable us to assess how and to what extent crustal volatiles liberate in natural magmas, a topic that is important for volcanic eruption dynamics, volatile budget and hazard mitigation.

PROJECTED PUBLICATIONS

The extensive dataset and visual representations of the analysed samples that has been achieved in this project are intended to contribute to publications on our wider xeno-pumice study coordinated by V.R. Troll. In addition, the textural information and quantitative measurements gained on the El Hierro samples in particular will likely form the basis for a separate publication on the vesiculation process of the El Hierro xeno-pumices, led by Berg, and which will form an integral part of her PhD thesis at Uppsala University.

REFERENCES

Abramoff, M. D., Magelhaes, P.J., & Ram, S.J., 2004. Image processing with ImageJ. *Biophotonics International*, 11, pp. 36–42.

Brun, F. and Dreossi, D., 2010. Efficient curve-skeleton computation for the analysis of biomedical 3D images. Biomedical Sciences Instrumentation, 46, pp. 475–480.

Brun, F., Mancini, L., Kasae, P., Favretto, S., Dreossi, D. & Tromba, G., 2010. Pore3D: A software library for quantitative analysis of porous media.*Nuclear Instruments and Methods in Physics Research, Section A: Accelerators, Spectrometers, Detectors, and Associated Equipment*, v. 615, pp. 326–332.

Cashman K.V. & Mangan M.T., 1994. Physical aspects of magmatic degassing II. Constraints on vesiculation processes from textural studies of eruptive products. In Carroll, M. R and Holloway, J. R. (Editors) Volatiles in magmas. *Reviews in Mineralogy 30*, pp. 447–478.

Hildebrand, T. and Rüegsegger, P., 1997. A new method for the model independent assessment of thickness in three-dimensional images. Journal of Microscopy, 185(1), pp. 67–75.

Hurwitz, S. & Navon, O., 1994. Bubble nucleation in rhyolitic melts: Experiments at high pressure, temperature, and water content. *Earth and Planetary Science Letters 122*, pp. 267-280.

Lindquist, W.B. and. Lee, S.M., 1996. Medial axis analysis of void structure in three-dimensional tomographic images of porous media. Journal of Geophysical Research, 101(84), pp. 8297–8310.

Ohser J. and Schladitz, K., 2009. 3D images of materials structures: processing and analysis. Wiley-VCH, Weinheim.

Perona, P. and Malik, J., 1990. Scale space and edge detection using anisotropic diffusion. IEEE Transactions on Pattern Analysis and Machine Intelligence, 12(7), pp. 629–639.

Soille, P., 2004. Morphological Image Analysis: Principles and Applications. Springer, Berlin, Heidelberg, 2nd edition.

Sparks, R. S. J., 1978. The dynamics of bubble formation and growth in magmas: a review and analysis. *Journal of Volcanology and Geothermal Research 3*, pp. 1-37.

Troll, V. R., Klügel, A., Longpré, M.-A., Burchardt, S., Deegan, F. M., Carracedo, J. C., Wiesmaier, S., Kueppers, U., Dahren, B., Blythe, L. S., Hansteen, T., Freda, C., Budd, D. A., Jolis, E. M., Jonsson, E., Meade, F., Berg, S., Mancini, L., and Polacci, M., 2012. Floating stones off El Hierro, Canary Islands: xenoliths of pre-island sedimentary origin in the early products of the October 2011 eruption., Solid Earth, 3, pp. 97–11.